Oxidative Dimer Formation Is the Critical Rate-Limiting Step for Parkinson's Disease α-Synuclein Fibrillogenesis†

Sampathkumar Krishnan,‡ Eva Y. Chi,§ Stephen J. Wood,|| Brent S. Kendrick,|| Cynthia Li,|| William Garzon-Rodriguez,‡ Jette Wypych,|| Theodore W. Randolph,§ Linda O. Narhi,|| Anja Leona Biere,|| Martin Citron,|| and John F. Carpenter*,‡

Department of Pharmaceutical Sciences, School of Pharmacy, University of Colorado Health Sciences Center, Denver, Colorado 80262, Department of Chemical Engineering, University of Colorado, Boulder, Colorado 80309, and Amgen, Inc., Thousand Oaks, California 91320

Received July 26, 2002; Revised Manuscript Received October 17, 2002

ABSTRACT: Intraneuronal deposition of α-synuclein as fibrils and oxidative stress are both implicated in the pathogenesis of Parkinson's disease. We found that the critical rate-limiting step in nucleation of α-synuclein fibrils under physiological conditions is the oxidative formation and accumulation of a dimeric, dityrosine cross-linked prenucleus. Dimer formation is accelerated for the pathogenic A30P and A53T mutant α-synucleins, because of their greater propensity to self-interact, which is reflected in the smaller values of the osmotic second virial coefficient compared to that of wild-type synuclein. Our finding that oxidation is an essential step in α-synuclein aggregation supports a mechanism of Parkinson's disease pathogenesis in which the separately studied pathogenic factors of oxidative stress and α-synuclein aggregation converge at the critical step of α-synuclein dimer formation.

Aggregation of α-synuclein and its deposition as fibrils in intracellular inclusions (e.g., Lewy bodies) are implicated in the pathogenesis of Parkinson's disease (PD)[1] and several other neurodegenerative diseases, including dementia with Lewy bodies (DLB), multiple-system atrophy, and the Lewy body variant of Alzheimer's disease (*1*). Two autosomal dominant mutations in α-synuclein (A53T and A30P) cause familial, early-onset PD (*1*−*3*). In α-synuclein transgenic mice and fruit flies, accumulation of intraneuronal α-synuclein deposits is associated with loss of dopaminergic neurons and with motor impairments (*4*−*7*).

Oxidative stress has long been invoked in the pathogenesis of PD (*8*). More recently, specific mediation of cellular damage via oxidation of α-synuclein has been proposed (*9*−*12*), and nitrated α-synuclein has been found in Lewy bodies of PD patients and in lesions of several other synucleinopathies (*11*, *12*). Furthermore, exposure of neuronal cells, overexpressing human α-synucleins, to oxidative conditions increases their vulnerability to this stress and promotes aggregation of α-synucleins (*10*, *13*−*15*).

In vitro, recombinant α-synucleins form fibrils that are similar ultrastructurally to those found in Lewy bodies (*16*−*18*). This aggregation is accelerated for the pathogenic A53T and A30P α-synucleins, suggesting that accelerated α-synuclein fibril formation may contribute to the early onset of familial PD (*16*−*18*). Patients with idiopathic PD express wild-type α-synuclein, which aggregates more slowly in vitro (*16*−*18*). However, applied oxidative and nitrative stresses in vitro rapidly induce dityrosine cross-linked aggregates and fibril formation of this protein, further supporting a critical role for oxidation in the initiation and/or progression of synucleinopathies (*19*−*21*).

Fibril formation by α-synucleins is a nucleation-dependent assembly process in which there is a characteristic lag phase followed by a rapid fibril growth phase (*22*, *23*). However, to date no study has addressed the surprising observation that—in the absence of artificial stresses such as agitation, stirring, or very low pH—the lag phases for α-synuclein fibril formation are extremely long (several weeks), yet highly reproducible across sample replicates (*18*, *22*, *23*). In a supersaturated solution, in which nuclei are formed directly from the parent molecules, nucleation is a stochastic event that should result in heterogeneity in time-dependent nucleation between samples (*24*). We recently proposed that for systems such as α-synuclein, lag phases are long and nonrandom because the rate-limiting step for the process is the formation and accumulation of a prenuclear species, which could be produced as a result of chemical processes with defined rates such as oxidation (*24*). As demonstrated with formulations of recombinant therapeutic proteins in aqueous solutions, protein oxidation can occur readily during long-term incubation even in the absence of an applied oxidative stress; molecular oxygen and/or metals from buffers are sufficient (*25*).

† Supported by National Science Foundation Grant BES 0138595 to J.F.C. and T.W.R.

* To whom correspondence should be addressed: Department of Pharmaceutical Sciences, School of Pharmacy, University of Colorado Health Sciences Center, Denver, CO 80262. Phone: (303) 315-6074. Fax: (303) 315-6281. E-mail: john.carpenter@uchsc.edu.

‡ University of Colorado Health Sciences Center.

§ University of Colorado.

|| Amgen, Inc.

[1] Abbreviations: PD, Parkinson's disease; DLB, dementia with Lewy bodies; SE-HPLC, size exclusion high-performance liquid chromatography; SDS, sodium dodecyl sulfate; EDTA, ethylenediaminetetraacetic acid; TEM, transmission electron microscopy; 2D UV, second-derivative ultraviolet; SLS, static light scattering.

10.1021/bi026528t CCC: $25.00
Published on Web 12/20/2002

In the current study, we investigated the critical rate-limiting step for fibrillogenesis of α-synuclein and the role of oxidation in this process by incubating solutions of wild-type, A53T, and A30P proteins—without agitation or stirring and under physiological conditions of temperature, pH, and ionic strength—in buffer alone and in buffer supplemented with 5 mM methionine and 2 mM EDTA. Methionine serves as a competitive scavenger for reactive oxygen species, and EDTA chelates trace quantities of metals that might be present in the buffer solution. The levels of native protein and oligomers in the soluble fraction of samples were analyzed by size exclusion high-performance liquid chromatography (SE-HPLC), a high-resolution method that can quantify minute amounts of aggregated protein (i.e., ≥0.5%) and is commonly used in pharmaceutical studies of aggregation pathways for protein therapeutics (*26*). The presence of fibrils in incubated samples was confirmed with thioflavin T fluorescence (*26*).

To gain insight into the greater propensity of the A30P and A53T α-synuclein mutants to form fibrils compared to the wild-type protein, we compared overall tertiary structures using measurements of the hydrodynamic radius and the radius of gyration and second-derivative UV spectroscopy. Furthermore, we quantified the self-interaction forces for the mutants and wild-type proteins by measuring the osmotic second virial coefficient using static light scattering.

EXPERIMENTAL PROCEDURES

Materials. The α-synucleins were cloned, expressed in *Escherichia coli*, and purified as previously described (*18*, *22*). The proteins were assessed to be >98% pure on the basis of SDS−polyacrylamide gel electrophoresis, HPLC−MS, and MALDI-TOF mass spectrometry. All chemicals were purchased from Sigma-Aldrich Corp. (St. Louis, MO) and were reagent grade or better.

In Vitro α-Synuclein Fibrillogenesis. Protein solutions (2 mg/mL) were prepared in "buffer" [20 mM Tris, 120 mM KCl, and 0.02% sodium azide (pH 7.0) at 37 °C] alone or buffer with 2 mM EDTA and 5 mM methionine. Protein concentrations were determined spectrophotometrically using an extinction coefficient of 0.354 at 280 nm and a 1 cm path for a 0.1% solution (*18*). In one experiment with the A30P α-synuclein variant, buffer and 10 mM methionine with and without 2 mM EDTA were also tested. Solutions were pipetted into V-shaped polypropylene Eppendorf tubes, which were then sealed and incubated at 37 °C, without stirring or agitation. At each time point during the incubation, sample tubes were removed from the incubator and the protein solution was divided into aliquots for the various analytical methods. Fibril growth was monitored using thioflavin T fluorescence as previously described (*26*). Insoluble fibrils were removed by centrifugation. Levels and molecular masses of the monomer protein and soluble oligomers in the supernatant were quantified and characterized using an HP 1090 size exclusion high-performance liquid chromatography system (SE-HPLC) equipped with a diode array UV absorbance detector. A Tosohaas TSK GEL G2000SW_{XL} column was used, with a mobile phase containing 20 mM Tris and 120 mM KCl (pH 7) and a flow rate of 0.6 mL/min. The column eluate was monitored at 215 nm. Peak areas in the chromatogram were used to quantify the amounts of monomer and dimer.

Seeding of Unmodified α-Synuclein with Dimers. To prepare the dimers, A30P α-synuclein (2 mg/mL) was incubated with an equimolar concentration of peroxynitrite in buffer [20 mM Tris and 120 mM KCl (pH 7.0)]. Peroxynitrite was generated using the method outlined by Beckman et al. (*27*) using the reaction between sodium nitrite and sodium hydroxide in the presence of hydrochloric acid. The concentration of peroxynitrite was measured by its absorbance (extinction coefficient at 306 nm = 1670 M^{-1} cm^{-1}). The protein solution was incubated at 37 °C, without stirring and agitation, in V-shaped Eppendorf tubes. To determine dimer levels during incubation, samples were withdrawn and analyzed using SE-HPLC as described previously. After 3 h, dimers were at a level of 8% of the total protein. Then the solution was removed from the 37 °C incubator and placed in a Centricon system (10 000 MW cutoff) to wash away the peroxynitrite. The sample was centrifuged and buffer (without peroxynitrite) was used to bring the sample back to its original volume. This process was repeated three times. Afterward, the sample was centrifuged again to concentrate the protein. To test the effects of seeding with dimers, two identical sets of unmodified A30P α-synuclein solutions (2 mg/mL) were incubated at pH 7.0 and 37 °C for 3 days, during which time dimers were not detected. Then one set of samples was seeded with the concentrated solution of dimers (and residual monomers), which was prepared after peroxynitrite treatment, to give a final dimer concentration of 6 μM (4% of the total protein). The seeded and unseeded control samples were incubated at 37 °C for 7 days. Samples were withdrawn and analyzed using SE-HPLC and the thioflavin assay at regular intervals.

Structural Properties of Monomeric, Dimeric, and Fibrillar Species. A light scattering, viscosity, and refractive index triple detector (E-Z Pro Model 300 TDA, Viscotek) was used to determine molecular masses, radii of gyration, and hydrodynamic radii for the species eluting from the size exclusion column (*28*). To test for the presence of dityrosine (*29*), samples from the incubation experiment were diluted to 100 μg/mL and analyzed for intrinsic fluorescence (25 °C) with excitation at 320 nm using an Aviv model ATF 15 spectrofluorometer. To compare the tertiary structures of the monomeric and dimeric α-synucleins, second derivatives of the UV absorbance spectra were obtained from the HP1090 liquid chromatography system's diode array detector as previously described (*30*). The structure of the fibrils formed during incubation at 37 °C and pH 7.0 was studied by TEM (Philips CM-10). The sample was placed on a glow-discharged grid (460-thin bar copper mesh) and negatively stained using a 2% uranyl acetate solution. The samples were then air-dried prior to analysis at 50000−100000×.

Mass Spectrometric Analysis of Dityrosine Cross-Links. To prepare dimers, a 2 mg/mL solution of A30P α-synuclein in buffer was treated with peroxynitrite as described above. The protein was then acid hydrolyzed by incubation in 6 N HCl at 60 °C for 12 h. The acid-hydrolyzed samples were analyzed by reverse phase HPLC using an elution gradient from 5 to 80% acetonitrile in the presence of 0.1% trifluoroacetic acid. A C-8 column (Phenomenex), connected to an HP 1100 system equipped with diode array and fluorescence detectors, was used for the analysis. The fluorescence detector was used to identify specific hydrolysis products with dityrosine cross-links by monitoring the

emission at 415 nm (excitation wavelength of 280 nm), and these products were analyzed further using a Quattro Micromass electrospray mass spectrometer.

Osmotic Second Virial Coefficients. Protein interactions were characterized by the osmotic second virial coefficient, B_{22}, where the subscripts denote protein−protein interactions. B_{22} values were determined by static light scattering (SLS) with a Brookhaven light scattering system (Brookhaven Instrument Corp., Holtsville, NY), equipped with a vertically polarized solid-state laser (wavelength $\lambda_o = 523$ nm), a BI-200SM goniometer, and a BI9000AT correlator. The SLS instrument was calibrated with pure toluene before each experiment. To minimize scattering from dust, sample vials were washed thoroughly and dried in a dust-free vacuum chamber, toluene and buffers used during SLS experiments were filtered with 0.02 μm inorganic Anatop syringe filters, and all protein solutions were filtered with 0.2 μm cellulose acetate syringe filters. Disturbances from dust were further minimized by using the built-in statistical criterion of dust-rejection-ratio cutoff value of 1.3. Dialyzed α-synuclein was diluted to a series of protein concentrations, ranging from 0.3 to 3 mg/mL, for SLS experiments. The same buffer (see above) that was used for the fibrillogenesis experiments was employed in the SLS experiments. Refractive index increments (dn/dC) of α-synucleins were determined independently via on-line SE-HPLC light scattering and using a differential refractometer (*31*). BI-ZP Software from Brookhaven was used to collect light scattering intensity data. Each data point was the average of no fewer than 30 statistically consistent measurements.

For particles such as α-synuclein that is small compared to the wavelength of incident light (linear dimensions smaller than $\lambda_o/20$), scattering is isotropic and the Rayleigh equation is used to interpret SLS data (*32*):

$$\frac{KC}{R_\theta} = \frac{1}{M_w} + 2B_{22}C \qquad (1)$$

where C is the protein mass concentration (grams per milliliter), R_θ is the excess Rayleigh ratio, M_w is the molecular mass of the protein (grams per mole), and B_{22} is the osmotic second virial coefficient (cubic centimeters per mole per square gram). K is a constant calculated from the optical properties of the system:

$$K = \frac{4\pi^2 n_o^2 (\mathrm{d}n/\mathrm{d}C)^2}{N_A \lambda_o^4} \qquad (2)$$

where n_o is the refractive index of the solvent, dn/dC is the protein refractive index increment (milliliters per gram), N_A is Avogadro's number, and λ_o is the wavelength of incident laser light. R_θ values were determined by subtracting the background scattering from buffer alone. The scattering intensity at 90° was measured to determine B_{22}; scattering from other angles was also monitored to verify isotropic scattering from α-synuclein.

RESULTS AND DISCUSSION

α-Synuclein Fibrillogenesis under Physiological Conditions. We incubated solutions of wild-type, A53T, and A30P proteins—without agitation or stirring and under physiological conditions of temperature, pH, and ionic strength—in buffer alone and in buffer supplemented with 5 mM methionine and 2 mM EDTA. With each protein variant, there was an initial lag phase during which fibrils were not detected (Figure 1) but during which there was observed the appearance and time-dependent accumulation of an oligomeric species that eluted earlier on SE-HPLC than the 14.5 kDa monomer (Figure 1). On-line light scattering detection indicated that this species was a dimer, with a molecular mass of 29 kDa. Furthermore, analysis of incubated samples by SDS gel electrophoresis also showed a dimer, which was covalently cross-linked (Figure 2A). In addition to dimer formation, the slow decrease in the level of the monomeric protein during the initial lag phase is also due to the formation of two fragments that eluted after the monomeric protein on SE-HPLC (Figure 1, inset). On-line light scattering detection indicated that these fragments had molecular masses consistent with their formation by hydrolysis of monomeric α-synuclein at Asp119 (*33*). The fragment levels increased slightly in the soluble fraction of samples throughout the incubation period. Also the fragments were not detected in insoluble fibril fractions, and thus do not appear to participate in fibril formation.

With wild-type α-synuclein incubated in buffer alone, the dimer level increased to ~2% of the total protein population until day 15 of incubation. Then, there was a rapid loss of dimers until day 25, after which dimers were no longer detectable in the soluble fraction. SDS gel electrophoresis confirmed that dimers are present only in the insoluble fibril fraction (data not shown). Concomitant with the rapid loss of dimers starting at day 15, there was a rapid loss of monomeric protein and an increase in thioflavin T fluorescence, indicating that fibril nucleation and growth had occurred. Analysis of the insoluble fraction with transmission electron microscopy confirmed that the loss of soluble protein was due to the formation of fibrils (Figure 2B). Thus, the rate-limiting step in nucleation of α-synuclein fibrils is the formation and accumulation of a prenuclear species, the covalently cross-linked dimer.

The same fibril formation pathway was observed for the mutant A53T and A30P α-synucleins except that the initial appearance of dimers and their accumulation to a critical concentration (ca. 1.5%) occurred more rapidly than for the wild-type protein, as did the resultant nucleation of fibril growth (Figure 1). Therefore, more rapid fibril formation by the mutant proteins is due to their propensity to form covalently cross-linked dimers being greater than that of the wild-type protein.

For all three α-synuclein variants, incubation in the presence of solution conditions that reduce the level of protein oxidation slowed the appearance and accumulation of dimers and, hence, lengthened the lag times for fibril nucleation (Figure 1). To test the effects of a higher concentration of methionine and whether metal chelation was important in our experimental system, we incubated A30P α-synuclein with 10 mM methionine, with and without 2 mM EDTA (Figure 3). With both solutions, the appearance of the covalent dimer was greatly delayed until near the end of the incubation (day 32) and fibrils were not detected until day 37, when the dimer concentration had just reached the critical level. The results (Figures 1 and 3) demonstrate that inhibition of oxidation and covalent dimer formation inhibit

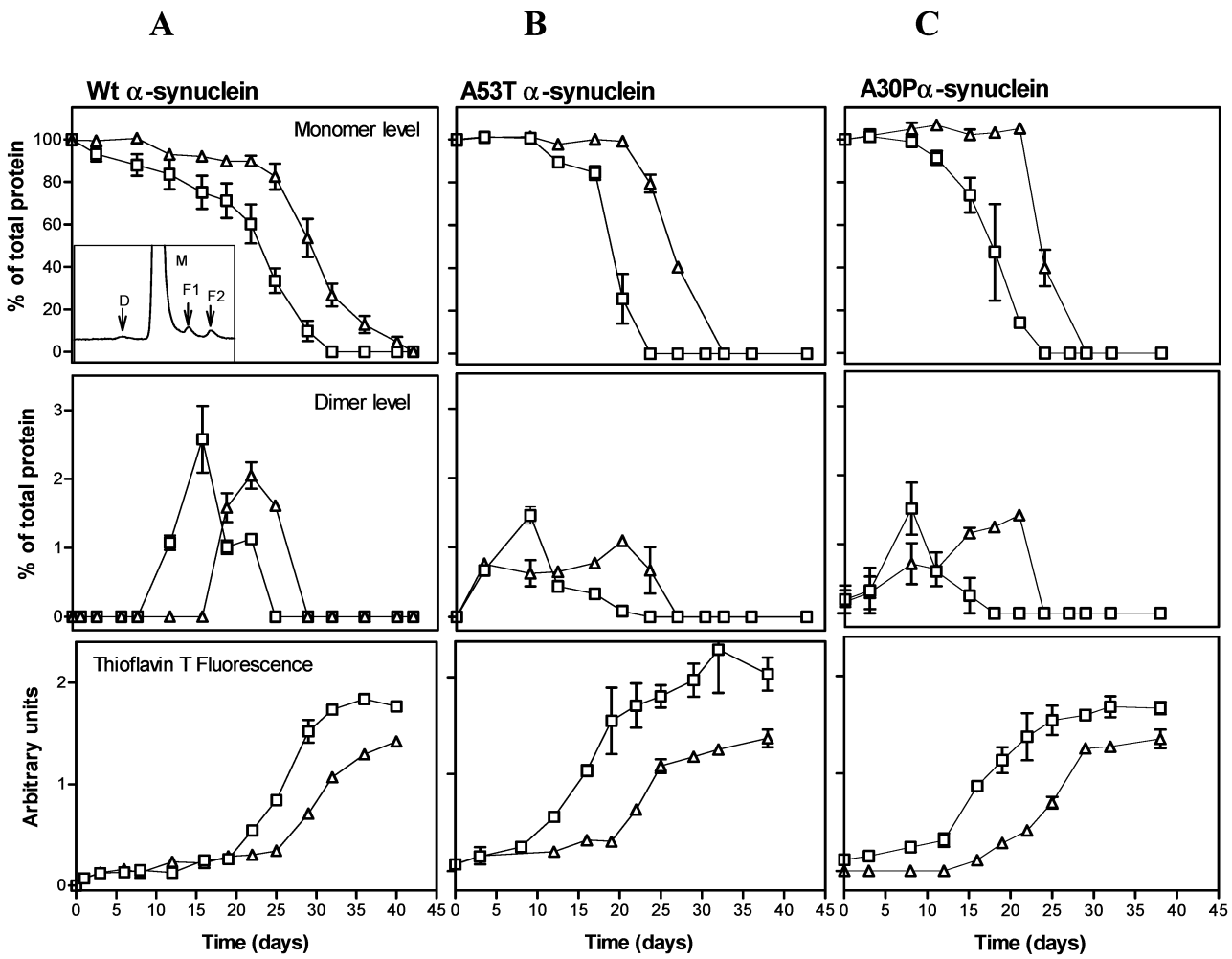

FIGURE 1: Levels of monomer (top panels), dimer (middle panels), and thioflavin T fluorescence (bottom panels) as a function of the time of incubation of (A) wild-type, (B) A53T, and (C) A30P α-synucleins. Results (means ± standard deviation for samples incubated in triplicate) are shown for protein solutions in buffer alone (□) or buffer with 2 mM EDTA and 5 mM methionine (△). The inset in panel A (top panel) shows a typical SE-HPLC chromatogram for an incubated sample in which peaks for the dimer (D), the monomer (M), and two fragments (F1 and F2) are shown.

α-synuclein fibril formation. Thus, in the absence of physical (e.g., agitation or stirring with Teflon bars, and/or exposure to high temperatures) or chemical (acid pH) stresses, oxidative formation of dimers is the critical, rate-limiting step for α-synuclein fibrillogenesis.

Seeding with Dimers Accelerates α-Synuclein Fibrillogenesis. To provide further evidence that dimer formation is the rate-limiting step for α-synuclein fibrillogenesis, we seeded an unmodified protein solution with dityrosine cross-linked dimers. The addition of dimers to unmodified A30P α-synuclein led to the rapid loss of the monomeric protein from solution due to fibril formation (Figure 4), compared to that in the unseeded control solution.

Intermolecular Dityrosine Cross-Link. How does oxidation lead to the covalent cross-link in α-synuclein dimers? In vitro exposure of wild-type α-synuclein to oxidation or nitration stresses induces formation of dimers and higher-order oligomers with dityrosine cross-links (*21*). α-Synuclein does not contain cysteine residues, and hence, covalent aggregate formation caused by oxidation is restricted to dityrosine cross-links. Dityrosine can be assessed with intrinsic fluorescence spectroscopy (*29*), a method that we applied to A30P α-synuclein samples as a function of the time of incubation in buffer at 37 °C. Concomitant with the increase in covalent dimer levels (Figure 2), there was an increase in fluorescence (excitation at 320 nm) emission intensity at ca. 420 nm (Figure 5A), which reflects the presence of dityrosine (*29*). As a function of incubation time, this peak shifts to a lower wavelength of 410 nm, closer to the signal observed for the protein that had been incubated in the presence of peroxynitrite for several hours. This blue shift in the signal suggests that the dityrosine cross-link is buried in a more hydrophobic environment, but the mechanism for this effect is currently not known. When fibrillogenesis led to protein precipitation and dimers were lost from the soluble fraction, there was a loss of the dityrosine fluorescence signal (data not shown). Thus, α-synuclein dimer formation in our studies is due to dityrosine cross-links, which occur more readily with the mutants than with the wild-type protein.

To further investigate the nature of the covalent linkage between dimers, peroxynitrite-treated A30P α-synuclein was acid hydrolyzed and analyzed with reverse phase HPLC. The chromatograms obtained with UV and fluorescence detection are shown in Figure 6. The fluorescence emission signal monitored at 415 nm (excitation wavelength of 280 nm), which is specific for detection of dityrosine residues, shows a strong peak for which only a small UV absorbance peak (280 nm) was observed in the chromatogram. Mass spec-

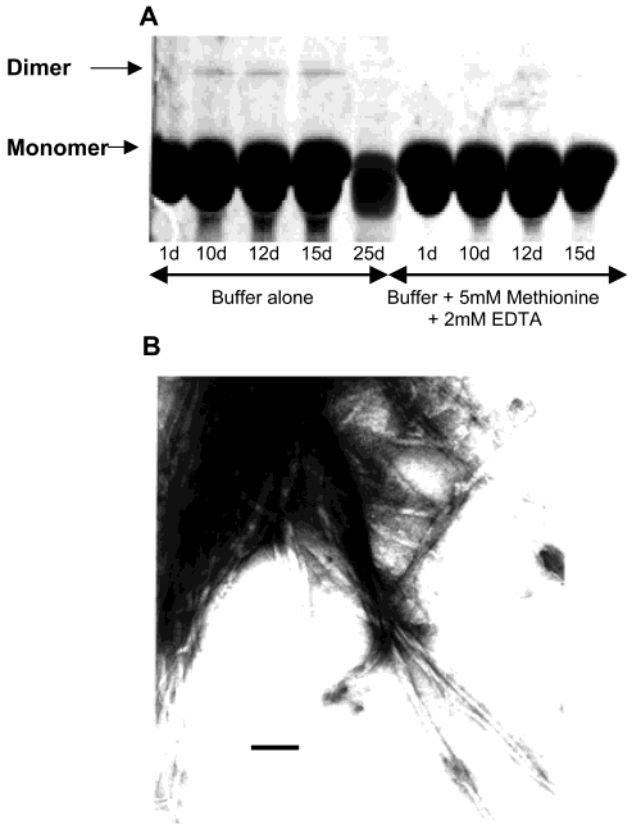

FIGURE 2: (A) SDS−PAGE analysis of the wild-type α-synuclein samples as a function of the time of incubation (samples were taken from the experiment described in the legend of Figure 1). The figure shows that dimers were present in the protein samples incubated in buffer alone (lanes 1−5) but not in the protein samples containing buffer with 5 mM methionine and 2 mM EDTA (lanes 6−9) for the first 15 days of incubation. (B) Transmission electron micrograph showing the fibrillar nature of aggregates of wild-type α-synuclein observed after 45 days of incubation under physiological conditions. A 100 nm scale bar is shown for comparison.

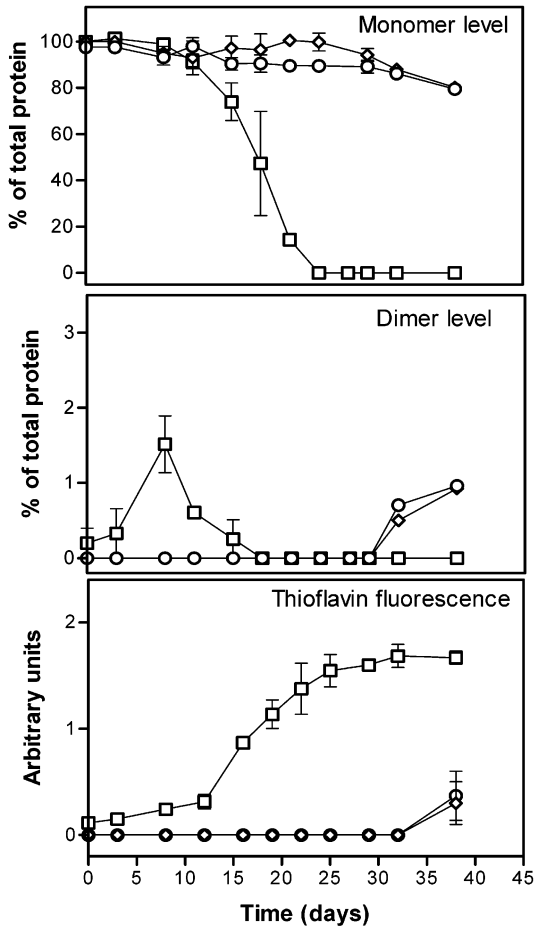

FIGURE 3: Levels of monomer (top panel), dimer (middle panel), and thioflavin T fluorescence (bottom panel) as a function of the time of incubation of A30P α-synuclein. Results (means ± standard deviation for samples incubated in triplicate) are shown for protein solutions in buffer alone (□), buffer with 10 mM methionine (○), and buffer with 10 mM methionine and 2 mM EDTA (◇).

trometry analysis of the hydrolysis product in this peak gave a mass of 359 ± 1.5 Da, which is consistent with the mass for dityrosine.

Increased Propensity of α-Synuclein Mutants To Form Dimers. What physicochemical property accounts for the propensity of the mutant α-synucleins to form dimers being greater than that of the wild-type protein? At neutral pH, all three α-synuclein variants have indistinguishable random coil secondary structure as determined by CD spectroscopy (*17*, *18*), and only slight differences between the variants are observed by NMR spectroscopy (*34*). All three variants are structurally expanded, as reflected in the relatively large (ca. 3 nm), but almost identical, hydrodynamic radii (R_h) for wild-type, A30P, and A53T α-synucleins (Table 1). In comparison, lysozyme, a typical globular protein with a comparable molecular mass (14.6 vs 14.5 kDa for α-synuclein), has a hydrodynamic radius of 2.05 nm (Table 1). R_h for completely unfolded lysozyme is 3.46 nm (*35*). Because R_h for each of the three α-synuclein variants is intermediate between the expected value for the compact, globular lysozyme and that for the completely unfolded lysozyme, the R_h data are consistent with α-synucleins adopting a partially structured conformation in solution. Consistent with this interpretation, the radii of gyration (R_g) indicate that each of the α-synuclein variants adopts a nonspherical structure in solution. For a sphere, the R_g/R_h ratio is predicted to be 0.775 (*35*). The ratio for lysozyme is 0.776, as expected for a nearly spherical molecule. In contrast, the R_g/R_h values for the wild type, A30P, and A53T are 0.99, 0.91, and 0.87, respectively. These ratios suggest that the time-averaged structure of the wild-type protein is more elongated than that for A53T, which appears to be slightly more globular. The values for the wild-type and A30P proteins are not statistically different (Table 1). The R_g/R_h ratios of dimeric species formed from wild-type, A30P, and A53T α-synuclein proteins, observed in the incubation study, were 0.93, 0.89, and 0.86, respectively. These results indicate that dimerization does not greatly alter the elongated structure of α-synucleins.

Second-derivative UV spectroscopy was also used to examine the tertiary structures of α-synuclein variants (*36*−*38*). The spectra of the wild-type and mutant α-synucleins are similar to the spectrum for *N*-acetyl tyrosinamide in buffer (Figure 5B), suggesting that the tyrosine residues in all of the α-synucleins that were tested are largely solvent exposed. These results are not surprising because three of the four tyrosine residues are found within 16 residues of the C-terminus, in a region that remains unordered even when the majority of the molecule adopts an α-helical conformation upon lipid membrane binding (*39*). Because of the high degree of solvent exposure of the tyrosine residues and an

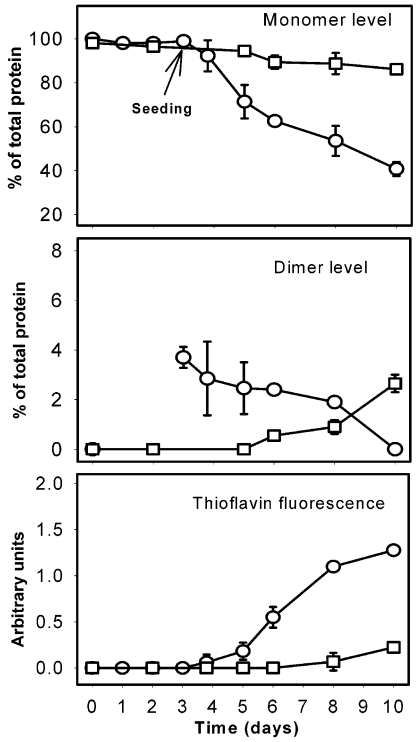

FIGURE 4: Levels of monomer (top panels), dimer (middle panels), and thioflavin T fluorescence (bottom panels) as a function of the time of incubation for seeded (○) and unseeded (□) A30P α-synuclein. Dimers (see Materials and Methods) were used to seed the sample after incubation for 3 days at 37 °C. Results are means ± standard deviation for samples incubated in triplicate.

implied high degree of conformational mobility in the disordered region, it is reasonable to expect that the formation of intermolecular dityrosine bonds would be minimally impeded by the structures of the α-synuclein variants.

Close examination of the second-derivative UV spectra does reveal a difference in the spectrum of A53T α-synuclein compared to those for the wild-type and A30P proteins. The minimum near 275 nm in the spectrum of the A53T mutant is red-shifted compared to those for the other two proteins by ∼1.4 nm (Figure 5B). Thus, although the tyrosine residues in all three variants are highly solvent exposed, those in the A53T α-synuclein are slightly less exposed than the tyrosine residues in the wild-type or A30P α-synuclein.

Figure 5B also shows the second-derivative UV spectrum of dimeric A30P α-synuclein. The tyrosine signals indicated by minima at 275 and 283 nm are strongly red-shifted relative to those of the monomeric species, suggesting that the tyrosine residues are much less solvent exposed in dimers than in monomers.

When the fact that structural constraints do not limit the capacity of dityrosine formation between α-synuclein molecules is considered, how can we explain the greater rates of dimer formation by the mutant α-synucleins? The osmotic second virial coefficient (B_{22}) is a solution thermodynamic parameter that provides insight into the different aggregation propensities of the α-synuclein variants. B_{22} directly reflects the strength of all protein−protein interactions on the molecular level, such as excluded volume, electrostatic, van der Waals, and all other short-range interactions. Positive values of B_{22} reflect overall repulsive interactions whereas negative B_{22} values reflect overall attractive interactions (*32*).

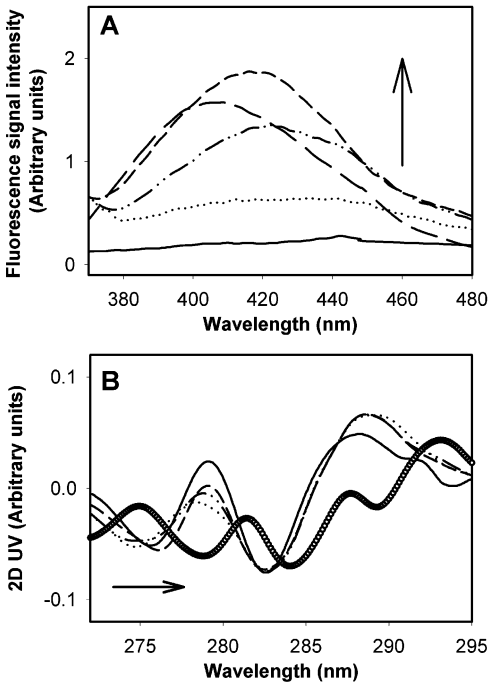

FIGURE 5: Structural properties of monomeric and dimeric α-synucleins. (A) Fluorescence emission spectra for A30P α-synuclein, as a function of the time of incubation in buffer alone at 37 °C. Samples from the experiment shown in Figure 3 were analyzed after incubation for 0 (—), 3 (•••), 5 (—••—), and 8 days (- - -). For comparison is shown the spectrum (— — —) for dimers purified by collecting SE-HPLC fractions from an A30P α-synuclein sample that was incubated in the presence of peroxynitrite, using a method previously shown (*21*) to induce dityrosine cross-links in α-synuclein. (B) Second-derivative UV spectra for native monomeric, wild-type (—••—), A53T (— — —), and A30P (•••) α-synucleins, and *N*-acetyl tyrosinamide (—). The spectrum for dimeric A30P α-synuclein is also shown (○). The UV absorbance spectrum was collected for the monomer peak on the SE-HPLC chromatogram using the HP1090s HPLC system's diode array detector (*36*). The direction of the arrows indicates the shift of the minima in the spectrum of the dimer with respect to the native protein.

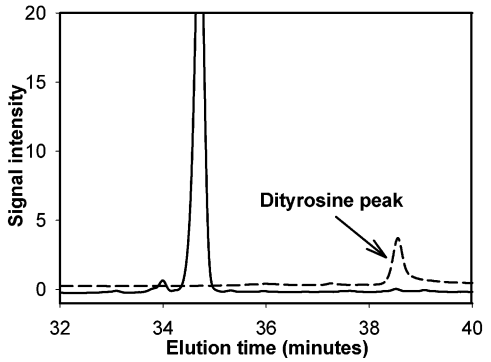

FIGURE 6: Reverse phase chromatograms of peroxynitrite-treated A30P α-synuclein after acid hydrolysis. Chromatograms are shown based on UV absorbance at 280 nm (—) and fluorescence emission at 415 nm when excited at 280 nm (— — —). The dityrosine peak is marked in the chromatogram.

B_{22} is fundamentally linked to solubility, and B_{22} measurements have been used to predict solution conditions for protein assembly into crystals and salting out (*32*, *40*−*43*) but have not been used previously to study protein aggregation. B_{22} values measured for wild-type, A30P, and A53T α-synucleins (Table 1) are positive, indicating overall

Table 1: Physical Properties of α-Synucleins

protein	osmotic second virial coefficient,[a] $B_{22} \times 10^3$ ($cm^3\ mol^{-1}\ g$)	radius of gyration of monomer,[b] R_g (nm)	hydrodynamic radius of monomer,[b] R_h (nm)	R_g/R_h
wild-type synuclein	5.64 ± 1.46[c]	2.94 ± 0.15	2.98 ± 0.07	0.98 ± 0.05[c]
A53T synuclein	1.94 ± 0.81[c]	2.76 ± 0.08	3.16 ± 0.19	0.87 ± 0.05[c]
A30P synuclein	2.94 ± 1.04	2.78 ± 0.07	3.07 ± 0.17	0.90 ± 0.05
lysozyme	not determined	1.59	2.05	0.77

[a] Standard deviations were obtained from errors in linear regression from slopes of Debye plots (eq 1). [b] Radii of gyration and hydrodynamic radii were determined using an on-line light scattering, viscosity and refractive index detector (E-Z Pro Model 300 TDA, Viscotek) connected to an SE-HPLC system (*28*). For a spherical molecule, $R_g/R_h = 0.775$ (*35*). Errors associated with R_g/R_h are propagated standard deviation errors. [c] Values are statistically different from each other on the basis of the paired *t* test ($p < 0.05$).

repulsive interactions, consistent with the long lag times observed for α-synuclein fibrillogenesis (Figure 1). However, B_{22} values for the A53T and A30P mutants are 48 and 66% smaller, respectively, than that for the wild-type protein. Thus, for both A53T and A30P, intermolecular forces for self-interaction are, on average, more attractive than those between wild-type molecules, a trend consistent with the increased capacity of the mutant α-synucleins to form dimers.

Because of their structural, functional, and surface anisotropy (*44*, *45*), protein−protein interactions are often dominated by the contributions of a relatively few, high-energy configurations rather than by overall colloidal interactions as described by the classic Derjaguin−Landau−Verwey−Overbeek (DLVO) theory (*45*). For example, a set of single-site mutations at a residue involved in a relatively weak crystal contact (S44) in lysozyme resulted in drastically different colloidal interaction behaviors (*44*). For some variants, these modified interactions were reflected in large increases in B_{22}, whereas other variants showed large decreases in B_{22}. The authors hypothesized that small changes in a protein may lead to significant changes in B_{22} when the changes occur in regions involved in high-complementarity interactions (*44*). Substitutions that modified the net charge of lysozyme had large effects on measured B_{22} values, with variants carrying greater charges (e.g., lysozyme S44K) exhibiting much larger B_{22} values (*44*). Steric perturbation, with the substitution of the bulkier residue phenylalanine, disrupted the complementarity of the original crystal contact but resulted in an increased complementarity in a different configuration involving the same residue; this secondary effect was reflected by a smaller measured value of B_{22} for lysozyme S44F (*44*).

This study offers interesting contrasts to the previous work on lysozyme variants. A30P and A53T α-synucleins are isocharged with respect to the wild type, so the smaller values of B_{22} for the variants, compared with that of the wild type, cannot be attributed to decreases in the extent of charge repulsion. Although both proline and threonine are bulkier than alanine, it is difficult to assign the decreased B_{22} values for A53T and A30P to steric disruption, since both the wild type and the variants exhibit highly expanded, random coil-like structures. It is possible that additional hydrogen bonding introduced by the more polar threonine in A53T contributes to smaller values of B_{22} than that for the wild type, but the same cannot be said for A30P. We hypothesize that the A53T and A30P substitutions introduce structural and dynamic changes in α-synuclein that result in increases in the strength and/or number of attractive intermolecular configurations.

Bussell and Eliezer observed with high-resolution NMR spectroscopy that the A30P mutation disrupts a region of residual α-helical structures that exist in wild-type α-synuclein whereas A53T shows a slight enhancement of a small region at the site of mutation with a preference for extended β-sheet conformations (*34*). Consistent with this result, our second-derivative UV spectra indicated that the level of solvent exposure of tyrosine residues was slightly lower in the A53T mutant than in the wild-type or A30P α-synuclein. Physiologically, α-synuclein has been hypothesized to play an important role in modulating synaptic plasticity (*39*, *46*). It binds reversibly to lipid membranes, and more interestingly, binding is accompanied by a dramatic increase in α-helicity from 3 to ∼80%, with a distinct distribution of polar and nonpolar residues on opposite faces of the induced α-helix structures (*39*, *46*−*49*). Because molten globules are often implicated as intermediates in protein aggregation pathways (*50*−*54*), we speculate that A30P and A53T mutations disrupt transient α-helix formation, resulting in a more globule-like conformation and an increased number of attractive self-interactions. Consistent with this idea, we find that the induction time for fibril formation correlates with R_g/R_h, with the most globular protein (A53T) having the shortest fibril formation induction time and the most attractive value for B_{22}, whereas the wild type is the least globular and has the longest induction time and the most repulsive value for B_{22}.

While the exact consequences of point mutations on protein structures and interactions are hard to predict, their effects are ultimately manifested in their solution behavior and captured in the experimentally measured B_{22}, as demonstrated by both α-synuclein and lysozyme variants. Numerous studies have revealed that a robust correlation exists between experimentally measured B_{22} values and protein solubility that extends over three decades of solubility for proteins with varied complexities (*42*, *55*, *56*). B_{22} is linked to protein equilibrium phase behavior, with the slightly negative B_{22} values that characterize crystallization conditions corresponding to a metastable liquid−liquid critical point in the vicinity of the liquid−solid equilibrium (*57*). In this metastable region, protein density fluctuations form small regions of high local protein concentration, followed by crystal nucleus formation and growth (*58*, *59*). Kulkarni and Zukoski in a recent study linked the strength of colloidal attraction to the rates of nucleation and found that the free energy barrier to the formation of a critical nucleus (or the induction time of protein crystal formation) is strongly correlated with B_{22} (*60*). Thus, the effect of the increased number of protein−protein attractive interactions (reflected in decreased B_{22} values) in A30P and A53T mutations is, on average, an increase in the local protein concentration. This higher fluctuating "local" protein concentration leads

to higher protein collision frequencies, which in turn leads to faster dimer formation. Because the rate-limiting step in nucleation of α-synuclein fibrils is the oxidative formation and accumulation of the dityrosine cross-linked dimer, a faster rate of dimer formation causes an earlier onset of fibril growth.

Conclusions. Our results document that oxidative dimer formation is the critical rate-limiting step for fibrillogenesis of α-synucleins and that the inherent propensity of the A30P and A53T mutant proteins to form dimers more readily accounts for their more rapid fibril formation. These data now firmly link oxidation and synuclein aggregation to the same pathogenic pathway. Our conclusions provide a direct mechanistic explanation for the arguments that impairments of cellular antioxidative mechanisms and/or overproduction of reactive species may be primary events in the initiation and progression of neurodegenerative synucleinopathies (*8*−*15*). Furthermore, elucidation of the role of oxidative and nitrative injury in mechanisms underlying these and other neurodegenerative disorders is crucial for identification of therapeutic targets for these diseases (*8*−*15*). Our in vitro system will be valuable for screening effective compounds, which should have the capacity to prevent, either directly or indirectly, the formation of oxidative dimers of α-synucleins.

ACKNOWLEDGMENT

We thank Carlos Catalano, Yong-Sung Kim, and Qin Yang for assistance with protein purification. Also a special thanks is due to Jean-Noel Lemercier for assistance with mass spectrometry.

REFERENCES

1. Galvin, J. E., Lee, V. M.-Y., and Trojanowski, J. Q. (2001) *Arch. Neurol. 58*, 186−190.
2. Polymeropoulos, M. H., Lavedan, C., Leroy, E., Ide, S. E., Dehejia, A., Dutra, A., Pike, B., Root, H., Rubenstein, J., Boyer, R., Stenroos, E. S., Chandrasekharappa, S., Athanassiadou, A., Papapetropoulos, T., Johnson, W. G., Lazzarini, A. M., Duvoisin, R. C., Di Iorio, G., Golbe, L. I., and Nussbaum, R. L. (1997) *Science 276*, 2045−2047.
3. Kruger, R., Kuhn, W., Muller, T., Woitalla, D., Graeber, M., Kosel, S., Przuntek, H., Epplen, J. T., Schols, L., and Riess, O. (1998) *Nat. Genet. 18*, 106−108.
4. Feany, M. B., and Bender, W. W. (2000) *Nature 404*, 394−398.
5. Masliah, E., Rockenstein, E., Veinbergs, I., Mallory, M., Hashimoto, M., Takeda, A., Sagara, Y., Sisk, A., and Mucke, L. (2000) *Science 287*, 1265−1269.
6. Van der Putten, H., Wiederhold, K.-H., Probst, A., Barbieri, S., Mistl, C., Danner, S., Kauffmann, S., Hofele, K., Spooren, W. P. J. M., Ruegg, M. A., Lin, S., Caroni, P., Sommer, B., Tolnay, M., and Bilbe, G. (2000) *J. Neurosci. 20*, 6021−6029.
7. Kahle, P. J., Neumann, M., Ozmen, L., Muller, V., Odoy, S., Okamoto, N., Jacobsen, H., Iwatsubo, T., Trojanowski, J. Q., Takahashi, H., Wakabayashi, K., Bogdanovic, N., Riederer, P., Kretzschmar, H. A., and Haass, C. (2001) *Am. J. Pathol. 159*, 2215−2225.
8. Beal, M. F. (1995) *Ann. Neurol. 38*, 357−366.
9. Butterfield, D. A., and Kanski, J. (2001) *Mech. Ageing Dev. 122*, 945−962.
10. Paxinou, E., Chen, Q., Weisse, M., Giasson, B. I., Norris, E. H., Rueter, S. M., Trojanowski, J. Q., Lee, V. M.-Y., and Ischiropoulos, H. (2001) *J. Neurosci. 21*, 8053−8061.
11. Giasson, B. I., Duda, J. E., Murray, I. V., Chen, Q., Souza, J. M., Hurtig, H. I., Ischiropoulos, H., Trojanowski, J. Q., and Lee, V. M.-Y. (2000) *Science 290*, 985−989.
12. Duda, J. E., Giasson, B. I., Chen, Q., Gur, T. L., Hurtig, H. I., Stern, M. B., Gollomp, S. M., Ischiropoulos, H., Lee, V. M.-Y., and Trojanowski, J. Q. (2000) *Am. J. Pathol. 157*, 1439−1445.
13. Zhou, W., Hurlbert, M. S., Schaack, J., Prasad, K. N., and Freed, C. R. (2000) *Brain Res. 866*, 33−43.
14. Ko, L., Mehta, N. D., Farrer, M., Easson, C., Hussey, J., Yen, S., Hardy, J., and Yen, S. H. (2000) *J. Neurochem. 75*, 2546−2554.
15. Ostrerova-Golts, N., Petrucelli, L., Hardy, J., Lee, J. M., Farer, M., and Wolozin, B. (2000) *J. Neurosci. 20*, 6048−6054.
16. Giasson, B. I., Uryu, K., Trojanowski, J. Q., and Lee, V. M.-Y. (1999) *J. Biol. Chem. 274*, 7619−7622.
17. Conway, K. A., Harper, J. D., and Lansbury, P. T., Jr. (1998) *Nat. Med. 4*, 1318−1320.
18. Narhi, L., Wood, S. J., Steavenson, S., Jiang, Y., Wu, G. M., Anafi, D., Kaufman, S. A., Martin, F., Sitney, K., Denis, P., Louis, J. C., Wypych, J., Biere, A. L., and Citron, M. (1999) *J. Biol. Chem. 274*, 9843−9846.
19. Hashimoto, M., Hsu, L. J., Xia, Y., Takeda, A., Sisk, A., Sundsmo, M., and Masliah, E. (1999) *Neuroreport 10*, 717−721.
20. Hashimoto, M., Takeda, A., Hsu, L. J., Takenouchi, T., and Masliah, E. (1999) *J. Biol. Chem. 274*, 28849−28852.
21. Souza, J. M., Giasson, B. I., Chen, Q., Lee, V. M.-Y., and Ischiropoulos, H. (2000) *J. Biol. Chem. 275*, 18344−18349.
22. Wood, S. J., Wypych, J., Steavenson, S., Louis, J. C., Citron, M., and Biere, A. L. (1999) *J. Biol. Chem. 274*, 19509−19512.
23. Conway, K. A., Lee, S.-J., Rochet, J.-C., Ding, T. T., Williamson, R. E., and Lansbury, P. T., Jr. (2000) *Proc. Natl. Acad. Sci. U.S.A. 97*, 571−576.
24. Kim, Y. S., Cape, S. P., Chi, E., Raffen, R., Wilkins-Stevens, P., Stevens, F. J., Manning, M. C., Randolph, T. W., Solomon, A., and Carpenter, J. F. (2001) *J. Biol. Chem. 276*, 1626−1633.
25. Hovorka, S. W., and Schöneich, C. (2001) *J. Pharm. Sci. 90*, 58−69.
26. Kim, Y., Wall, J. S., Meyer, J., Murphy, C., Randolph, T. W., Manning, M. C., Solomon, A., and Carpenter, J. F. (2000) *J. Biol. Chem. 275*, 1570−1574.
27. Beckman, J. S., and Koppenol, W. H. (1996) *Am. J. Physiol. 217*, C1424−C1437.
28. Wen, J., Arakawa, T., and Philo, J. S. (1996) *Anal. Biochem. 240*, 155−166.
29. Amado, R., Aeschbach, R., and Neukom, H. (1984) *Methods Enzymol. 107*, 377−388.
30. Krishnan, S., Chi, E. Y., Webb, J. N., Chang, B. S., Shan, D., Goldenberg, M., Manning, M. C., Randolph, T. W., and Carpenter, J. F. (2002) *Biochemistry 41*, 6422−6431.
31. Kendrick, B. S., Kerwin, B. A., Chang, B. S., and Philo, J. S. (2001) *Anal. Biochem. 299*, 136−146.
32. George, A., and Wilson, W. W. (1994) *Acta Crystallogr. D50*, 361−365.
33. Conway, K. A., Harper, J. D., and Lansbury, P. J., Jr. (2000) *Biochemistry 39*, 2552−2563.
34. Bussell, R., Jr., and Eliezer, D. (2001) *J. Biol. Chem. 276*, 45996−46003.
35. Wilkins, D. K., Grimshaw, S. B., Receveur, V., Dobson, C. M., Jones, J. A., and Smith, L. J. (1999) *Biochemistry 38*, 16424−16431.
36. Ackland, C. E., Berndt, W. G., Frezza, J. E., Landgraf, B. E., Pritchard, K. W., and Ciardelli, T. L. (1991) *J. Chromatogr. 540*, 187−198.
37. Mach, H., and Middaugh, C. R. (1994) *Anal. Biochem. 222*, 323−331.
38. Servillo, L., Colonna, G., Balestrieri, C., Ragone, R., and Irace, G. (1982) *Anal. Biochem. 126*, 251−257.
39. Davidson, W. S., Jonas, A., Clayton, D. F., and George, J. M. (1998) *J. Biol. Chem. 273*, 9443−9449.
40. George, A., Chiang, Y., Guo, B., Arabshahi, A., Cai, Z., and Wilson, W. W. (1997) *Methods Enzymol. 276*, 100−110.
41. Guo, B., Kao, S., McDonald, H., Asanov, A., Combs, L. L., and Wilson, W. W. (1999) *J. Cryst. Growth 196*, 424−433.
42. Haas, C., Drenth, J., and Wilson, W. W. (1999) *J. Phys. Chem. B 103*, 2808−2811.
43. Pjura, P. E., Lenhoff, A. M., Leonard, S. A., and Gittis, A. G. (2000) *J. Mol. Biol. 300*, 235−239.
44. Chang, R. C., Asthagiri, D., and Lenhoff, A. M. (2000) *Proteins: Struct., Funct., Genet. 41*, 123−132.
45. Neal, B. L., Asthagiri, D., and Lenhoff, A. (1998) *Biophys. J. 75*, 2469−2477.
46. Jo, E., McLaurin, J., Yip, C. M., George-Hyslop, P. S., and Fraser, P. E. (2000) *J. Biol. Chem. 275*, 34328−34334.
47. Eliezer, D., Kutluay, E., Robert Bussell, J., and Browne, G. (2001) *J. Mol. Biol. 307*, 1061−1073.

48. McLean, P. J., Kawamata, H., Ribich, S., and Hyman, B. T. (2000) *J. Biol. Chem. 275*, 8812−8816.
49. Narayanan, V., and Scarlata, S. (2001) *Biochemistry 40*, 9927−9934.
50. Betts, S., HassePettingell, C., and King, J. (1997) *Adv. Protein Chem. 50*, 243−264.
51. Fink, A. L. (1998) *Folding Des. 3*, R9−R23.
52. Kendrick, B. S., Carpenter, J. F., Cleland, J. L., and Randolph, T. W. (1998) *Proc. Natl. Acad. Sci. U.S.A. 95*, 14142−14146.
53. Webb, J. N., Webb, S. D., Cleland, J. L., Carpenter, J. F., and Randolph, T. W. (2001) *Proc. Natl. Acad. Sci. U.S.A. 8*, 7259−7264.
54. Wetzel, R. (1994) *Trends Biotechnol. 12*, 193−198.
55. Rosenbaum, D. F., Kulkarni, A., Ramakrishnan, S., and Zukoski, C. F. (1999) *J. Chem. Phys. 111*, 9882−9890.
56. Farnum, M., and Zukoski, C. (1999) *Biophys. J. 76*, 2716−2726.
57. Rosenbaum, D., Zamora, P. C., and Zukoski, C. F. (1996) *Phys. Rev. Lett. 76*, 150−153.
58. Haas, C., and Drenth, J. (1999) *J. Cryst. Growth 196*, 388−394.
59. Curtis, R. A., Blanch, H. W., and Prausnitz, J. M. (2001) *J. Phys. Chem. B 105*, 2445−2452.
60. Kulkarni, A. M., and Zukoski, C. F. (2002) *Langmuir 18*, 3090−3099.

BI026528T